Journal of Power Sources 195 (2010) 5573–5580

Contents lists available at ScienceDirect

Journal of Power Sources

journal homepage: www.elsevier.com/locate/jpowsour

Fluorinated carboxylic membranes deposited by plasma enhanced chemical vapour deposition for fuel cell applications

J. Thery[a,*], S. Martin[b], V. Faucheux[a], L. Le Van Jodin[b], D. Truffier-Boutry[a], A. Martinent[a], J.-Y. Laurent[a]

[a] Laboratory of Printed Component, LITEN, CEA Grenoble, 17 rue des martyrs, 38054 Grenoble Cedex 09, France
[b] Laboratory of Components for the Micro-storage of Energy, LITEN, CEA Grenoble, 17 rue des martyrs, 38054 Grenoble Cedex 09, France

ARTICLE INFO

Article history:
Received 5 January 2010
Received in revised form 6 March 2010
Accepted 8 March 2010
Available online 12 March 2010

Keywords:
Ion conductive membrane
Plasma
Chemical vapour deposition
Proton exchange membrane fuel cell

ABSTRACT

Among the fuel cell technologies, the polymer electrolyte membrane fuel cells (PEMFCs) are particularly promising because they are energy-efficient, clean, and fuel-flexible (i.e., can use hydrogen or methanol). The great majority of PEM fuel cells rely on a polymer electrolyte from the family of perfluorosulfonic acid membranes, nevertheless alternative materials are currently being developed, mainly to offer the alternative workout techniques which are required for the portable energy sources. Plasma polymerization represents a good solution, as it offers the possibility to deposit thin layer with an accurate and homogeneous thickness, even on 3D surfaces. In this paper, we present the results for the growth of proton conductive fluoro carboxylic membranes elaborated by plasma enhanced chemical vapour deposition. These membranes present conductivity values of the same order than the one of Nafion®. The properties of the membrane, such as the chemical composition, the ionic conductivity, the swelling behaviour and the permeability were correlated to the plasma process parameters. The membranes were integrated in fuel cells on porous substrates and we present here the results regarding the barrier effect and the power output. Barrier effect similar to those of 40 μm Nafion® layers was reached for 10 μm thick carboxylic membranes. Power outputs around 3 mW cm^{-2} were measured. We discuss the results regarding the gas barrier effect and the power outputs.

1. Introduction

Because of carbon dioxide emission issues, the dependence on fossil fuels can no longer be tolerated and the need for commercial renewable energy solutions becomes crucial [1]. In order to drop the carbon dioxide emissions, it is essential to decrease the energy, but in parallel, using non-carbon energies appears incontrovertible. Fuel cells are potential emerging technologies for clean energy, and particularly polymer electrolyte membrane fuel cells (PEMFCs) appear as a promising candidate because they are efficient, clean, fuel-flexible [2]. Regarding the carbon dioxide emission, the vehicles and stationary power market are often pointed up, but fuel cells are reaching commercial viability sooner in other applications such as portable displays such as laptops, cell phones, games [3–6] aiming at filling out the ability of batteries to power these mobile devices for extended periods of time. Indeed, the scope regarding the cost of power for portable electronics is more flexible than for cars market. However, engineering the compact fuel cells needed for these systems is not easy and technological challenges still remain. Technologies such as thin film deposition, etching and lithography techniques could provide a solution to that problem but the classical fuel cells material have to be reconsidered. Regarding the catalytic electrodes, solutions such as platinum sputtering present quite positive result [7,8]. Regarding the ionic membrane, ion conductive PECVD thin films have been widely studied [9–26]. They present adequate characteristics to have low ionic specific resistance and simultaneously, to act as barrier against the gas diffusion. Since elevated cross-linking density can be obtained with PECVD techniques, very low gas permeability can be reached. Moreover, since low thickness membranes can be grown, low specific resistance can be reached, even with quite low ionic conductivity. Until now, the great majority of proton exchange membranes work thanks to hydrated perfluorosulfonic acid (PSA) membranes [27]. PSA is a copolymer of tetrafluoroethylene (TFE) and various perfluorosulfonate monomers. Nafion®, which is manufactured by Dupont, is perhaps the most widely known PSA. These membranes present an excellent chemical and mechanical stability, as well as elevated proton conductivity [28] (around 130 mS cm^{-1}). They are constituted of a polytetrafluoroethylene hydrophobic (PTFE) backbone with perfluorinated vinyl-polyether side chains containing hydrophilic sulfonic acid end groups. The presence of both hydrophilic and hydrophobic functionalities on a

* Corresponding author. Tel.: +33 4 3878 1940; fax: +33 4 3878 5117.
E-mail address: jessica.thery@cea.fr (J. Thery).

0378-7753/$ – see front matter
doi:10.1016/j.jpowsour.2010.03.019

same polymeric chain leads to an organisation into nano-domains [29] and these last are responsible for the great proton conductivity of the hydrated Nafion®. Indeed, the water absorption induces a modification of the micro-structure. When the water content is increased, the structure moves from spherical isolated ionic clusters to spherical ionic domains connected with cylinders of water. When exposed to water, the SO_3H groups are hydrolyzed into $SO_3^-H^+$, allowing for an effective proton transport across the membrane. The migration of hydrated protons [$H^+H_2O_n$ species] is thus supported [30] and the proton conductivity is increased. To create similar membranes with plasma enhanced chemical vapour deposition (PECVD), the majority of researchers tried to reproduce this combination of hydrophilic/hydrophobic nano-domain. The goal of such an approach is to decrease the proton resistance whether by increasing the proton conductivity or by decreasing the membrane thickness. Commonly, the membranes result from the reaction of an acidic fluorinated precursor, with a carbonated or fluorocarbonated monomer. Nevertheless, since the acidic group is weak, to prevent from their destruction, low plasma powers leading to low growth rates are required. Mex et al. [21–23] proposed a fluorocarbon membrane with phosphonic acid groups, from the plasma polymerization of vinyl phosphonic acid and tetrafluoroethylene and measured surprising conductivities as high as 1500 mS cm^{-1} (at 80 °C). Brault [26] and Roualdes et al. [24,25] developed fluorocarbon membranes with sulfonic acid groups, with conductivities varying from 10^{-5} mS cm^{-1} to 10^{-1} mS cm^{-1}.

This article deals with the synthesis of ion conductive membranes by plasma enhanced chemical vapour deposition. The approach presented in this article breaks with the conventional approach. Instead of preserving the acidic groups with low plasma power, the acidic functions are directly created in the plasma. We present here the process for the growth of ionic conductive carboxylic films, the relation between the process parameters and the properties of the films. The as-grown membranes were integrated in fuel cells and their performances were measured via OCV (Open Circuit Voltage) measurements and polarization curves. The results are shown to be strongly correlated with the deposition process parameters, and the film thickness. Barrier effect similar to that of 40 μm Nafion® layers was reached for 10 μm thick carboxylic membranes and maximal power outputs around 3 mW cm^{-2} were measured.

2. Experimental

2.1. Deposition of the membranes

The plasma polymerization was carried out using a capacitive-coupled reactor with a r.f. power supply of 13.56 MHz (see Fig. 1).

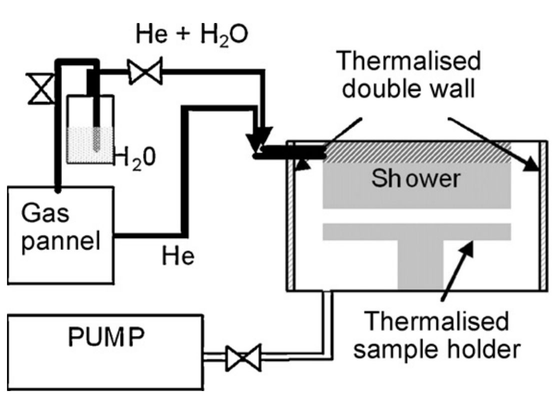

Fig. 1. Scheme of the PECVD reactor used for the CFO growth. The H_2O flow is controlled via the helium flow.

The radio frequency (r.f.) power is delivered by a Dressler Cesar 1310 generator to the showerhead-type upper electrode. An oil jacket is used to maintain the reactor walls at 328 K. Vacuum is made by a dry two-stage Alcatel ADS601 pumping system. Pressure is measured via MKS Baratron® gauges and controlled by a VAT throttle valve system. A base pressure of 10^{-3} mbar was reached before each deposition. The water was vapourized at 50 °C and vapours were carried by inert helium from a thermostatic bubbler to the chamber. The ionic membranes were grown from the plasma polymerization of water vapour with C_4F_8. For this study, the plasma power was varied between 50 W and 500 W. The water flow was controlled by changing the helium flow from 0 sccm to 180 sccm.

2.2. Characterization methods

The plasma was characterized by Optical Emission Spectroscopy (OES). Measurements were performed via a quartz optical fibre. The spectral line intensities were recorded by means of an Avantes monochromator (3600 grooves mm^{-1}).

The chemical composition was determined from Fourier Transform InfraRed (FT-IR) spectra and X-ray Photoelectron Spectroscopy (XPS) analysis. FT-IR spectra were obtained by using a Thermo electron-Nicolet type Nexus 870 in the range of 4000–400 cm^{-1}. The XPS analyses were made with an Axis NOVA (Kratos) model, using a monochromatic AlKα source. Before each XPS measurement, the sample surface was etched with Ar^+ ions sputtering.

The thickness of the films and the refractive index were measured by spectroscopic ellipsometry in the range of 240–840 nm with a SOPRA GES5 ellipsometer. A Cauchy dispersion is used to describe the refractive index profiles of the films.

The fuel cells were observed via Field Emission Scanning Electron Microscopy (FE-SEM) images, with a Hitachi S4100 model.

The ionic conductivity of the membranes was measured in the film plane by impedance spectroscopy with a Solartron apparatus in the range of 1 MHz to 0.1 Hz. The films were deposited on glass substrates with platinum blocking electrodes. As the conductivity strongly depends on the humidity rate, measurements were made in a home-made climatic chamber under a saturated humidity rate to prevent from weather forecast effects. Before each conductivity measurement, we waited the stability of the resistance from 0.5 h to 3 h, depending on the film. To validate the in-plane value, we measured the same conductivity for a standard Nafion® membrane. For a 30 μm thick Nafion® layer, in-plane conductivity between 120 mS cm^{-1} and 150 mS cm^{-1} was found.

The polarization curves were measured with a VMP3 (biologic and Co.) in galvano cyclic mode. Before each measurement, the OCVs were stabilized for 10 min. The tests were performed at room temperature, in ambient conditions.

2.3. Realization of the fuel cells

The 0.8 cm^2 fuel cells were directly manufactured on a ceramic porous substrate with thin film deposition techniques (see Fig. 2b). The various layers composing these micro fuel cells are presented schematically in Fig. 2a. The gold collectors were deposited via sputtering techniques and the catalytic layers were deposited via spraying a C/Pt ink [31]. The substrates used were porous ceramic substrates. Fig. 3 presents the hydrogen flow as a function of the hydrogen pressure, for substrates with pores sizes varying between 2 μm and 20 μm. Since ceramic substrates with smaller pores are not commercially available, substrates with 2 μm pores were chosen. Indeed, with peak to valley roughness around 4 μm (see Table 1), these substrates are the smoothest. In addition, for hydrogen pressures of 400 Pa over the atmospheric pressure, they allow

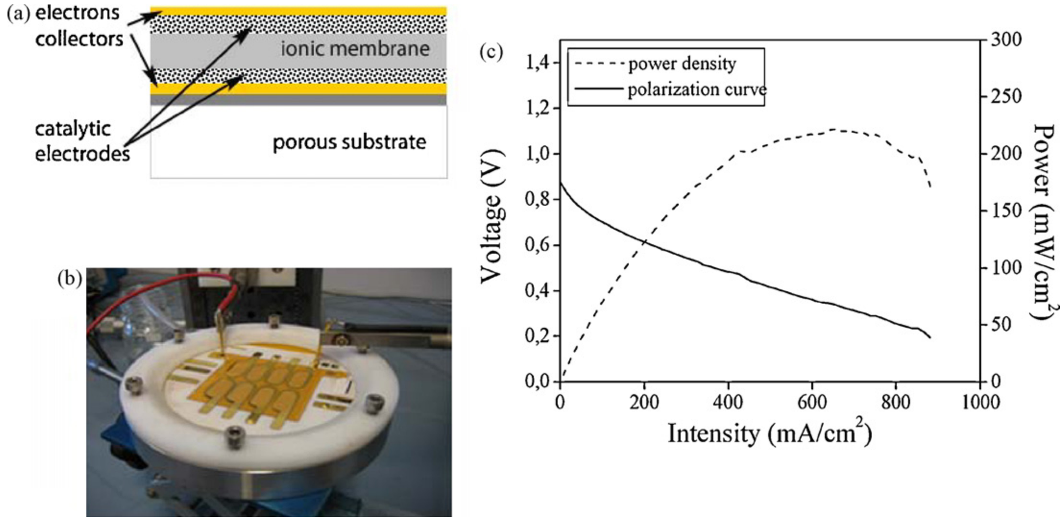

Fig. 2. (a) Scheme of the fuel cell stack. (b) Testing device with eight fuel cells – each fuel cell has a surface of 0.8 cm^2. (c) Polarization curve and corresponding power output for a fuel cell with a 30 μm thick Nafion® membrane, tested at a H_2 pressure of 1000 Pa over the atmospheric pressure.

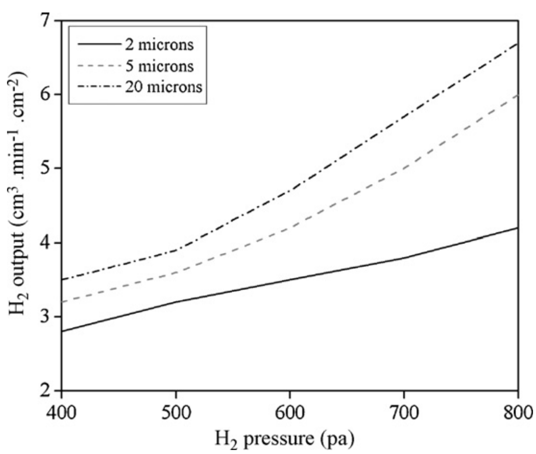

Fig. 3. Hydrogen flow as a function of the hydrogen pressure (above the atmospheric pressure), for ceramic substrates with pores sizes varying between 2 μm and 20 μm.

a hydrogen flow of 2.8 cm^3 (min^{-1} cm^{-2}) which is "sufficient" to drive 370 mA cm^{-2}.

In order to have a reference, we deposited a fuel cell using a Nafion® membrane as electrolyte. Such a stack gave reproducible OCV as high as 950 ± 50 mV and polarization curves leading to 220 mW cm^{-2} (see Fig. 2c).

3. Results and discussion

3.1. Plasma process and correlation with the membrane properties

The growth rate was found to depend on the plasma power, as shown in Fig. 4a. Below 400 W, the growth rate varies linearly with the r.f. power. The rise in the deposition rate with the r.f. power can be explained by the increase of the plasma density. For the r.f. powers superior to 400 W, the growth rate reaches a threshold, meaning that it is limited by the precursor amount. The growth rate was also found dependent from the water flow (see Fig. 4a) as the rise of the water flow leads to a decreased growth rate. We assume that the radicals resulting from the water decomposition participate in an etching mechanism. Fig. 4b shows the variation

Table 1
Peak to valley roughness for various ceramic substrates.

Average pore size (μm)	PV roughness (μm)
2	3.8
5	7
20	25

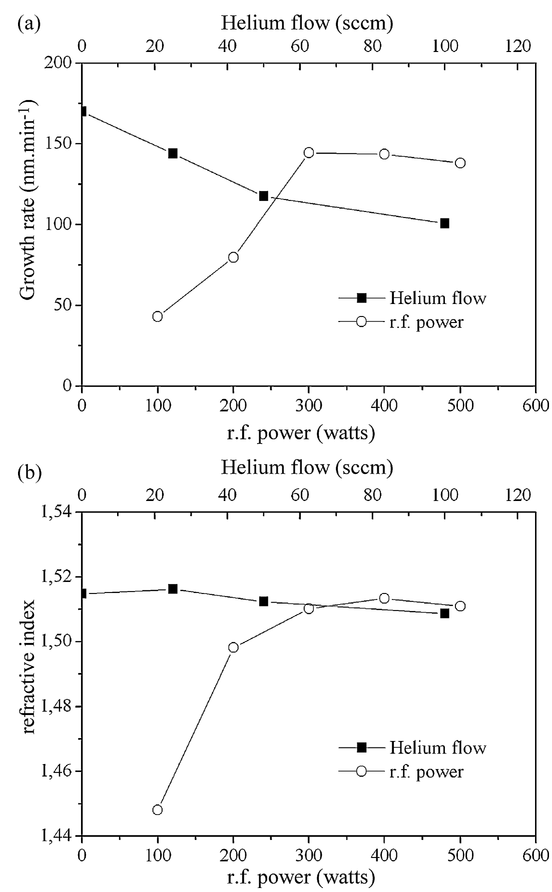

Fig. 4. (a) Growth rate of the carboxylic membrane as a function of the plasma power and the helium flow. (b) Refractive index of the carboxylic membranes as a function of the plasma power and the helium flow. For the impact of the r.f. power, the helium flow was fixed at 25 sccm and for the impact of the helium flow, the r.f. power was fixed at 300 W.

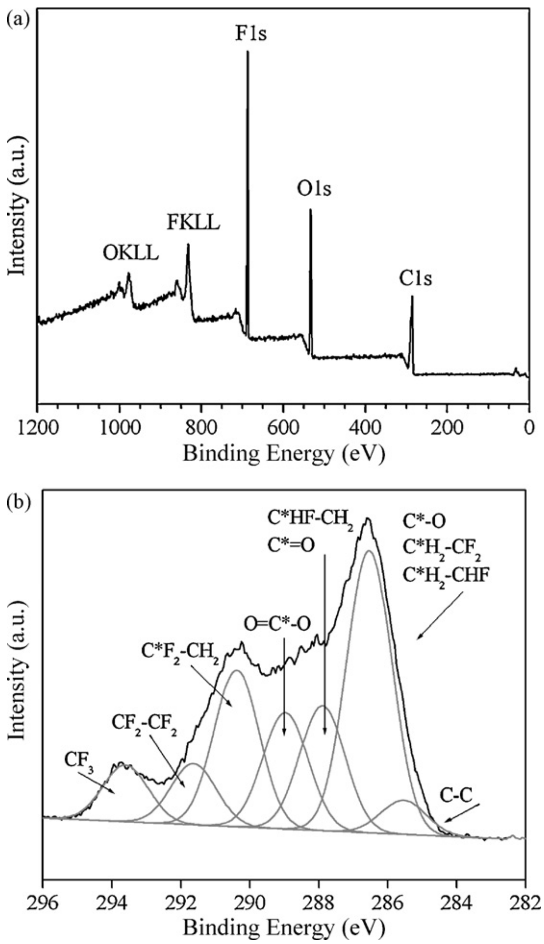

Fig. 5. XPS spectra of a carboxylic membrane with a conductivity of 80 mS cm^{-1}. (a) The survey spectra. (b) The C1s environment.

of the refractive index of the as-grown layer as a function of the r.f. power and the bubbling helium flow. As the plasma power was increased, the refractive index of the films was also raised, meaning that the high r.f. power films are denser. Also, the as-grown thin films may have a high cross-linking density with increasing r.f. power [32,33]. Regarding the influence of the bubbling helium flow, the refractive index is slightly decreased but on the whole, the films density seems mainly controlled by the r.f. power.

The chemical composition of the films was analysed via FT-IR and XPS analyses. The analysis of the C1s, F1s and O1s peaks reveals the presence of C–C, C=C, C–H, CH_2–CF_x, C–O, CF–CF_2, C=O, CF–CF_3, O–C=O, CF_2, CF_2–CF_2, CF_3, CF, CF_2 and CF_3 bonds (see Fig. 5). Fig. 6 presents typical FT-IR spectra for CFO conductive films. The main groups are C_x–F_y, C=O and O–H. Considering both analyses, we assume that the CFO films are formed by a C_xF_y matrix with carboxylic, ketone and aldehyde functionalities.

OES has established that adding water to the C_4F_8 plasma leads mainly to OH and CO emissions. Fig. 7 compares the optical emission spectra for a C_4F_8 and a C_4F_8/H_2O r.f. discharge (P = 1 mbar and Pe = 200 W). For the C_4F_8 discharge, the CF_x band emission [34] is observed in a wavelength range from 300 nm to 400 nm. The band at wavelengths above 500 nm is the second order spectrum of the CF_x band emission. The emission of fluorine F and carbon C_2 molecules are very weak compared with the CF_x band. Adding water to the C_4F_8 monomer leads to a clear OH emission around 308 nm indicating that H_2O is dissociated by means of $H_2O \rightarrow OH + H$. Since no oxygen atoms could be detected, we assume that they recombine immediately or are ionized into O^{2+} ions. According to these observations, we assume that the formation of the carboxylic groups results mainly from the oxidation of the C_4F_8 co-monomer by OH, resulting in fluoride ketone or aldehyde and fluoride carboxylic acids formation.

$$\left.\begin{array}{l}[C_xF_y]_n + OH \rightarrow [C_xF_{y-1}OH] + F \\ [C_xF_{y-1}OH] + OH \rightarrow C_xF_{y-2}O + F + H_2O \\ C_xF_{y-2}O + OH \rightarrow C_{x-1}F_{y-3}COOH + F\end{array}\right\} \text{ carboxylic groups formation}$$
$$C_{x-1}F_{y-3}COOH + OH \rightarrow C_{x-1}F_{y-3} + CO_2 + H_2O$$

We studied the influence of the growth parameters on the chemical composition and the ionic conductivity of the membranes. Fig. 6 presents the FT-IR spectra as a function of the plasma powers and the bubbling helium flows. Low plasma power and high water flows favour elevated C=O/CF ratio, which characterizes the density of carboxylic functions with respect to the fluorocarbonated chains. At the same time enhanced conductivities were measured for the elevated C=O/CF ratio (see Fig. 6a). We think that for the highest plasma power, the oxidation of the C_4F_8 molecules into CO_2 is favoured and leads to low carboxylic groups density. In the end, conductivities of the same order than the one of the Nafion® membranes were reached for plasma power Pe < 200 W. The acidic dissociation for the carboxylic groups is much lower than for the sulfonic acids and consequently, these elevated conductivities were not expected. We assume that it can be correlated to a huge density of COOH groups. This was evaluated through the measurement of the Ion Exchange Capacity (IEC) of the membrane. The IEC was determined by an exchange of acidic protons with another cation in solution [35]. For CFO membranes with conductivities ranging from 70 mS cm^{-1} to 100 mS cm^{-1}, IEC between 2.2 mequiv. g^{-1} and 3 mequiv. g^{-1} were measured. In comparison, Nafion® 2021 membranes present an IEC of 0.9 mequiv. g^{-1}.

The swelling behaviour directly reflects the ability to absorb water and is thus closely linked to the ionic conductivity. The swelling behaviour of a 70 mS cm^{-1} conductive membrane was evaluated with the method of dynamic vapour sorption (DVS) [36]. Fig. 8 compares the water uptake of a carboxylic membrane and a standard Nafion® 212 membrane. With a mass uptake around 18%, the CFO membrane is quite similar to a Nafion® membrane.

3.2. Integration of the membrane in fuel cell stacks

The carboxylic membranes were integrated in fuel cells varying parameters such as the r.f. power (from 50 W to 500 W), the water flow (through the bubbling helium flow which varied from 0 sccm to 100 sccm) and the membrane thickness (from 1 μm to 30 μm).

Fig. 9 shows the evolution of the OCV as a function of the r.f. power for 10 μm thick membranes. The "low plasma power" films (Pe < 100 W) present a huge gas crossover that lead to short circuit of the fuel cells (OCV = 0 mV). These important leaks can be related to the low cross-linking degree of these films. Indeed, for the PECVD films, the degree of cross-linking reduces when the r.f. power decreases [32,33]. This weak reticulation leads to a lack of cohesion and thus a membrane with numerous nanometrics defects. For enhanced plasma powers (Pe > 100 W), as the cross-linked functionalities density is increased, positive OCV could be measured. The largest OCV of 600 mV is measured for plasma powers at around 300 W, and a further increase of the r.f. power did not allow rising the OCV (Fig. 9). Consequently, even for strongly reticulated membranes, the gas diffusion is not as low as the one measured for 30 μm thick Nafion® membranes. We assume that for r.f. powers below 300 W, increasing the power enhances the intrinsic permeability. Beyond 300 W, the permeation through the membrane can no longer be correlated to the material's intrinsic permeability but rather to micro-structural defects.

For a 300 W film, we also studied the influence of the membrane thickness on the gas barrier behaviour. Fig. 9 shows that

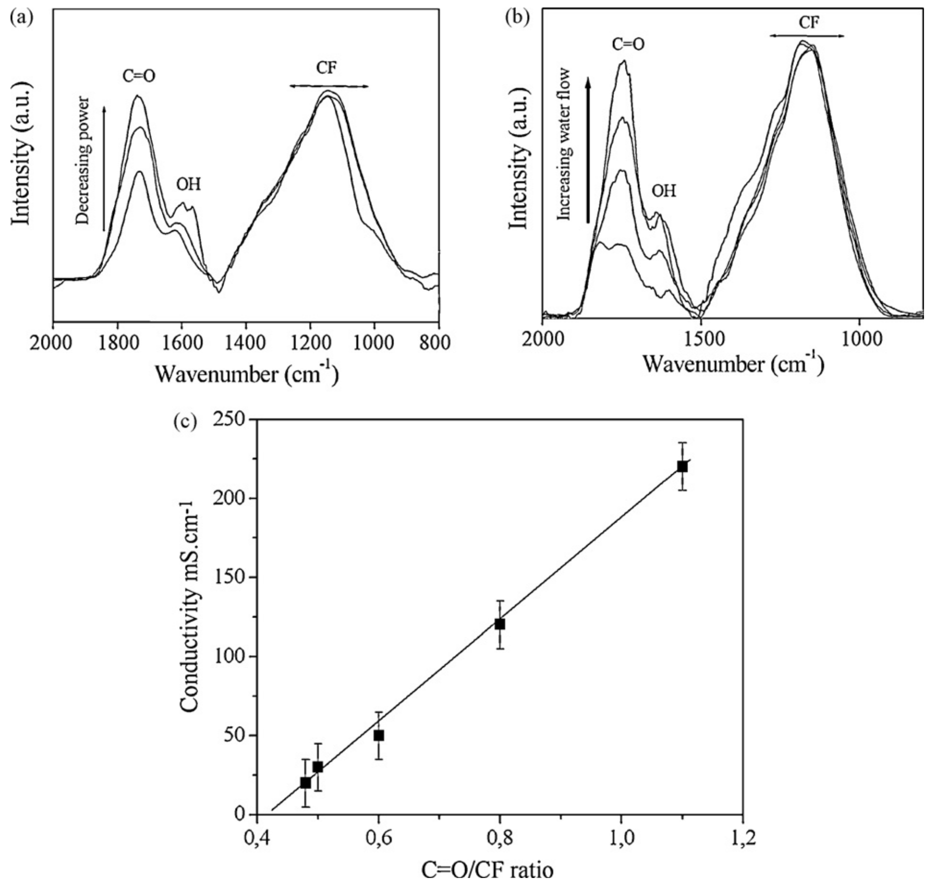

Fig. 6. (a) Impact of the plasma power on the FT-IR spectra: the plasma power varies between 100 W and 400 W, the helium flow is fixed at 100 sccm. (b) Impact of the water flow on the FT-IR spectra, the helium flow varies between 0 sccm and 100 sccm, the plasma power is fixed at 200 W. (c) Variation of the ionic conductivity as a function of the C=O/CF ratio. The C=O/CF ratio is defined as the intensity ratio between the respective FT-IR peaks.

for thicknesses inferior to 10 μm, the OCV depends on the membrane thickness. However, from thicknesses of 10 μm, the OCV reaches the limit of 600 mV. We assume therefore that 10 μm is the critical thickness to cover the defects generated by the substrate roughness [37]. For thicknesses superior to 10 μm, micro-structural defects cannot be avoided even by increasing the membrane thickness. These defects are responsible for the hydrogen diffusion through the membrane. They may result from stresses in the film or be generated during the film growth by defects at the substrate surface. Consequently, neither the film reticulation nor the film thickness could allow sufficient gas barrier effect, on our porous substrates.

To by-pass these problems of crossing defects, multilayer coatings were grown. The layer superposition can in fact afford to manage the intrinsic defects by bringing more complex diffusion pathways due to an atomic rearrangement at the multilayer interfaces [38–40]. The procedure to obtain multilayer consisted in stopping the growth and resetting the atmospheric pressure in the chamber before the growth of the N + 1 layer. The ionic conductivity perpendicular to the film plane was not affected by the interfaces. Fig. 10 presents the effect of the number of layers on

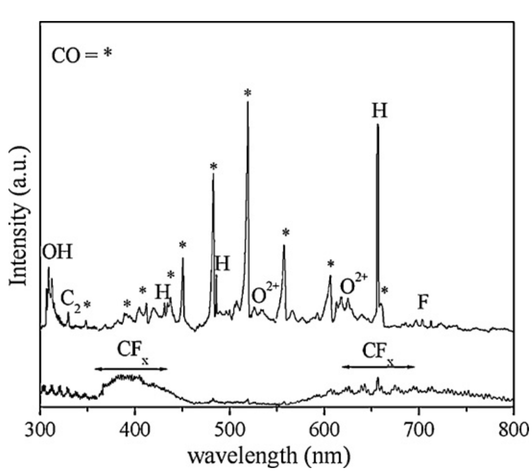

Fig. 7. OES spectra of the C_4F_8 r.f. discharge (below) and the $C_4F_8 + H_2O$ discharge.

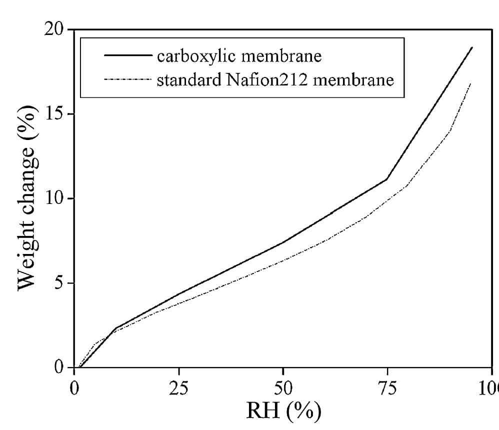

Fig. 8. Mass uptake of the ion conductive membrane as a function of the humidity rate for a CFO film compared to a standard Nafion® film.

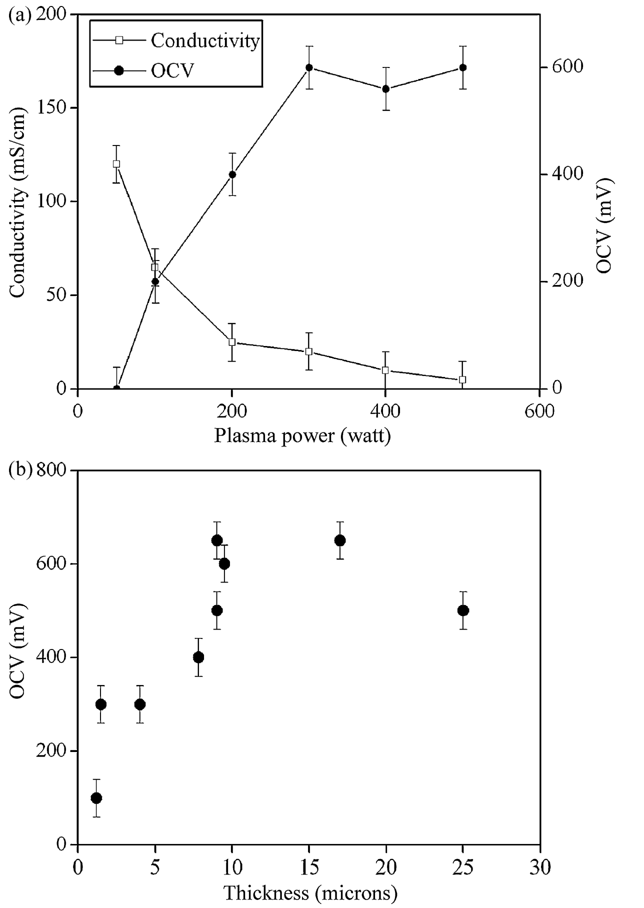

Fig. 9. (a) Influence of the plasma power on the OCV and on the ionic conductivity. (b) Evolution of the OCV as a function of the membrane thickness.

the OCV and shows that four layers are sufficient to reach OCV of 900 mV, meaning that micrometrics defects no longer cross the membrane. Thereby, multilayers afford to reach permeation level as low as those of a 30 μm Nafion® membrane with a decreased thickness of 10 μm. Since very thin and highly cross-linked membranes can be grown thanks to PECVD techniques, previous works pointed out that the PECVD membranes could provide a solution for decreased specific resistances and enhanced barrier effect [12,41]. Our work underlines parameters that have to be considered to achieve performing fuel cells. First of all, it has to be kept in mind

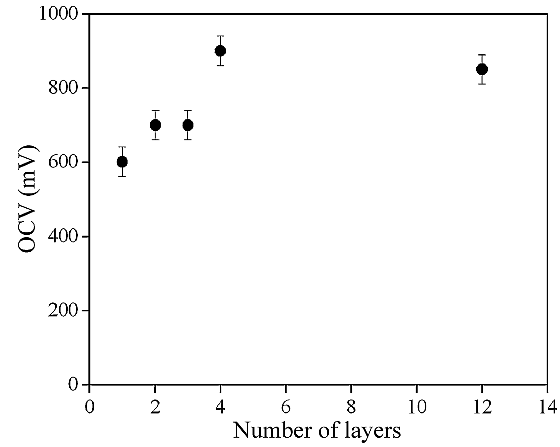

Fig. 10. Impact of the interfaces' number on OCV for 10 μm thick membranes.

that the membrane's thickness is dependant from the substrate roughness. Theoretically, one can imagine flat porous substrates, but these are not common and the porous substrate commercially available (yarn, porous ceramic, porous graphite substrates) are quite rough. We showed that for substrates with PV roughness of 4 μm, the membrane thickness is at least of 10 μm. If we consider the actual Nafion® coatings, thicknesses of 30 μm can easily be reached. Consequently, even though the vacuum techniques allow the deposition of thin membranes with a decreased permeability, there is a lack of smooth and stiff porous substrates that could allow the growth of thin permeable ionic membranes.

In order to estimate the behaviour of the membrane more practically, multilayers coatings were integrated in fuel cells. Fig. 11 presents the polarization curve for a 300 W multilayered membrane, with a total thickness of 10 μm and an ionic conductivity of 10–30 mS cm^{-1}. The power output was measured via polarization curves and the best results obtained are of about 3 mW cm^{-2}. This result is quite low compared with the 220 mW cm^{-2} measured for a fuel cell with a 30 μm thick Nafion® layer. We assume that this result is correlated to the low ionic conductivity for the 300 W films. Indeed, if the 300 W films are optimal in terms of cross-linking density, they present a poor ionic conductivity. In that case, even if the thickness is decreased by a factor of three, the carboxylic films still present specific ionic resistances around $10^{-5}\,\Omega\,cm^2$ whereas the Nafion® membranes show ionic resistances around $2 \times 10^{-6}\,\Omega\,cm^2$. In order to increase the conductivity while preserving elevated plasma powers, we may increase the water flow (see Fig. 6). Ten microns cross-linked multilayered membranes were

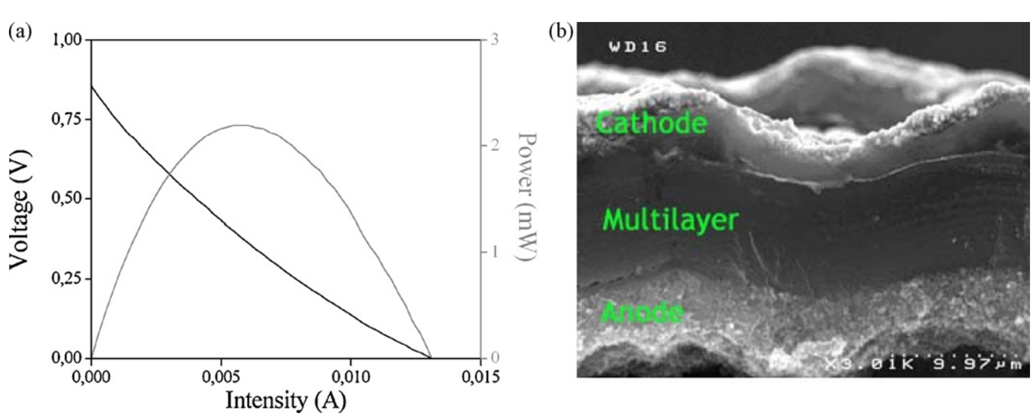

Fig. 11. (a) Polarization curve for a multilayer coating with a thickness around 10 μm, with a layers' number of 12 and a conductivity around 20 mS cm^{-1}. (b) SEM cross section of the corresponding fuel cell.

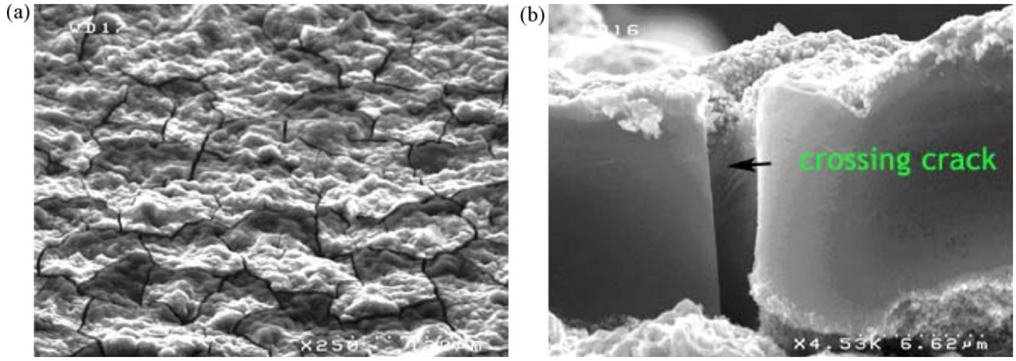

Fig. 12. SEM picture of the fuel cell post moistening: (a) surface view and (b) cross section view.

thus grown, with a measured conductivity around 70 mS cm^{-1} (and thus a specific ionic resistance of $2 \times 10^{-6}\ \Omega\ cm^2$). Nevertheless, no OCV could be detected for such a stack, and evidence of a very huge crossover was pointed out. The SEM analyses revealed the presence of numerous cracks, crossing the entire membrane thickness (see Fig. 12). The membranes were observed before and after water immersion. Before immersion, no cracks were detected. After immersion, numerous cracks were noticed, showing that the cracks appear during the membrane swelling.

This observation raises another issue, relative to the mechanical behaviour of the PECVD membranes. Indeed, the ionic membranes swell and the swelling is proportional to the ionic conductivity. Consequently, the proton conductive material must be resilient to bear the expected deformation. Satterfield et al. [42] studied the mechanical properties of Nafion® membranes and found an elastic modulus around 300 MPa at room temperature. The plastic modulus of Nafion® is almost independent of the temperature below Tg (Tg ≈ 110 °C) with a value of 8–10 MPa. With a Young modulus inferior to 5 GPa, Nafion® is thus a compliant material. Regarding the carboxylic membranes, we showed that an important cross-linking is required for an effective barrier effect. Nevertheless, in such conditions, the membranes are rigid and cannot deform without cracking. One can reasonably wonder about the ability of PECVD films to be flexible enough to sustain the water swelling. Generally speaking, the PECVD thin films are not known for their resilience. For example, the fluorocarbon PECVD films, called "Teflon like" coatings show much higher hardness (of the order of GPa) than the corresponding Teflon coatings (young modulus around 500 MPa), even if the wetting properties are similar [43]. Indeed, the mechanical properties are closely related to the molecules chain length and to their ability to move. Since plasma processes are very destructive with regard to the precursor monomers, highly reticulated films are deposited. The chain length is consequently limited and the chains are immobilized due to numerous covalent bonds. In addition, for the proton conductive membranes in hand in this article, the conductivity is related to the density of –COOH groups. Nevertheless for elevated conductivities, a huge –COOH density is required, leading thus to very short chains.

In order to get resilient membranes, we will have to change from amorphous cross-linked networks to linear perfluorinated chain. Large molecular chains will be favoured and thus low density of acidic groups. For this purpose, the sulfonic groups seem more adapted since huge conductivities may be reached with a lower density of acidic functionalities. In addition, to favour the formation of large chains, one may prefer a soft plasma chemistry. Introducing a pulsed modulation to the r.f. discharge may allow a greater variability in monomer fragmentation and thus to approach true plasma polymerization. Finally, the precursor formulation should allow middle chain groups that could provide flexibility such as ether segments.

4. Conclusions

In short, we have deposited fluorinated carboxylic membranes with ionic conductivities as high as the one of perfluorosulfonic acid membranes. We showed that the membranes properties are strongly coupled with the growth parameters. Ionic conductivity superior to 100 mS cm^{-1} is measured for low plasma power films. Nevertheless, for those low r.f. powers, the film reticulation is weak and the intrinsic permeation through the membrane is huge. In order to optimize the gas barrier effect, we found that cross-linked membranes are required. Considering our precursors flows, r.f. powers above 200 W are required. We found a compromise between conductivity and reticulation, and cross-linked films with conductivity around 70 mS cm^{-1} were grown. Since rough substrates are used, we found that a critical thickness of 10 μm is required to reach low permeation level, even with highly reticulated films. For 10 μm thick cross-linked membrane, the permeation level does not reach the one of the Nafion® coatings. This is due to the presence of crossing defects induced by the roughness at the substrate's surface. In the end, growing multilayered membrane allowed to reach the low permeation level researched. With multilayer coatings, one can reach the same permeation level as the one of a 30 μm thick Nafion® membrane. OCV around 900 mV was measured for fuel cell with a 10 μm thick carboxylic membrane, with a conductivity of ~20 mS cm^{-1}. Two kinds of reticulated multilayered membranes were integrated in fuel cells. The membrane with a conductivity of about 20 mS cm^{-1} allowed OCV of 900 mV and power output around 3 mW cm^{-2}, whereas the membranes with increased conductivities of 70 mS cm^{-1} cracked while water swelling. We assume that these membranes showed too low resilience to sustain the deformation induced during swelling.

Acknowledgements

This work has been supported by the European Commission through the sixth and the seventh Framework Program for Research and Technological Development, with the NAPOLYDE project, -2005-515846 and the SMALLINONE project, -2008-2.6.1, which addresses the NMP thematic area "Novel material for energy applications". We also thank G. Gebel for the water uptake measurements.

References

[1] H.V. Storch, N. Stehr, Nature 405 (2000) 615.
[2] C.E. Health, A.G. Revfsz, Science 180 (1973) 542.
[3] L.C.D. Baertsch, K.F. Jensen, J.L. Hertz, H.L. Tuller, S.T. Vengallatore, S.M. Spearing, M.A. Schmidt, J. Mater. Res. 19 (2004) 2604.
[4] Z.P. Shao, S.M. Haile, J. Ahn, P.D. Ronney, Z.L. Zhan, S.A. Barnett, Nature 435 (2005) 795.
[5] D. Nikbin, Fuel Cell Rev. 3 (2006) 21.

[6] D. Beckel, A. Bierberle-Hütter, A. Harvey, A. Infortuna, U.P. Mücke, M. Prestat, J.L.M. Rupp, L.J. Gauckler, J. Power Sources 173 (2007) 325.
[7] S. Hirano, J. Kim, S. Srinivasan, Electrochim. Acta 42 (1997) 1587.
[8] P. Brault, A. Caillard, A.L. Thomann, J. Mathias, C. Charles, R.W. Boswell, S. Escribano, J. Durand, T. Sauvage, J. Phys. D 37 (2004) 3419.
[9] Y. Uchimoto, K. Yasuda, Z. Ogumi, Z.-I. Takehara, J. Electrochem. Soc. 138 (1991) 3190.
[10] F. Finsterwalder, G. Hambitzer, J. Membr. Sci. 185 (2001) 105.
[11] P.D. Beattie, F.P. Orfino, V.I. Basura, K. Zichowska, J. Ding, C. Chuy, J. Schmeisser, S. Holdcroft, J. Electroanal. Chem. 503 (2001) 45.
[12] N. Inagaki, S. Tasaka, Z. Chengfei, Polym. Bull. 26 (1991) 187.
[13] N. Inagaki, S. Tasaka, Y. Horikawa, J. Polym. Sci. A: Polym. Chem. 27 (1989) 3495.
[14] N. Inagaki, S. Tasaka, T. Kurita, Polym. Bull. 22 (1989) 15.
[15] Z. Ogumi, Y. Uchimoto, K. Yasuda, Z.-I. Takehara, Chem. Lett. 953 (1990).
[16] Z. Ogumi, Y. Uchimoto, Z.-I. Takehara, J. Electrochem. Soc. 137 (1990) 3319.
[17] Y. Uchimoto, K. Yasuda, Z. Ogumi, Z.-I. Takehara, A. Tasaka, T. Imahigashi, Ber. Bunsenges. Phys. Chem. 97 (1993) 625.
[18] Y. Uchimoto, E. Endo, K. Yasuda, Y. Yamasaki, Z.-I. Takehara, Z. Ogumi, O. Kitao, J. Electrochem. Soc. 147 (2000) 111.
[19] K. Yasuda, Y. Uchimoto, Z. Ogumi, Z.-I. Takehara, J. Electrochem. Soc. 141 (1994) 2350.
[20] K. Yasuda, Y. Uchimoto, Z. Ogumi, Z.-I. Takehara, Ber. Bunsenges. Phys. Chem. 98 (1994) 631.
[21] L. Mex, J. Muller, Membr. Technol. 115 (1999) 5.
[22] L. Mex, N. Ponnat, J. Muller, Fuel Cell Bull. 4 (2001) 9.
[23] L. Mex, M. Sussiek, J. Muller, Chem. Eng. Commun. 190 (2003) 1085.
[24] S. Roualdes, I. Topala, H. Mahdjoub, V. Rouessac, P. Sistat, J. Durand, J. Power Sources 158 (2006) 1270.
[25] H. Mahdjoub, S. Roualdes, P. Sistat, N. Pradeilles, J. Durand, G. Pourcelly, Fuel Cells 5 (2005) 277.
[26] P. Brault, S. Roualdès, A. Caillard, A.-L. Thomann, J. Mathias, J. Durand, C. Coutanceau, J.-M. Léger, C. Charles, R. Boswell, Eur. Phys. J. Appl. Phys. 34 (2006) 151.
[27] S. Banerjee, D. Curtis, J. Fluor. Chem. 125 (2004) 1211.
[28] Y. Sone, P. Ekdunge, D. Simonsson, J. Electrochem. Soc. 143 (1996) 1254.
[29] A.-L. Rollet, O. Diat, G. Gebel, J. Phys. Chem. B 106 (12) (2002).
[30] T.A. Zawodzinski Jr., C. Derouin, S. Radzinski, R.J. Sherman, V.T. Smith, T.E. Springer, S. Gottesfeld, J. Electrochem. Soc. 140 (1993) 1041.
[31] Karst, et al., J. Power Sources (2009), doi:10.1016/j.jpowsour2009.08.068.
[32] S.-H. Cho, Z.-T. Park, J.-G. Kim, J.-H. Boo, Surf. Coat. Technol. 174–175 (2003) 1111–1115.
[33] S.M. Smith, S.A. Voight, H. Tompkins, A. Hooper, A.A. Talin, J. Vella, Thin Solid Films 398–399 (2001) 163.
[34] K.A. Blanks, K. Becker, J. Phys. B 20 (1987) 6157.
[35] T.-Y. Chen, J. Leddy, Langmuir 16 (2000) 2866.
[36] F.M. Collette, C. Lorentz, G. Gebel, F. Thominette, J. Membr. Sci. 330 (2009) 21–29.
[37] A.S. Da Silva Sobrinho, G. Gzeremuszkin, M. Latrèche, G. Dennler, M.R. Wertheimer, Surf. Coat. Technol. 116–119 (1999) 1204.
[38] G. Dennler, C. Lungenschmied, H. Neugebauer, N.S. Sariciftci, M. Latrèche, G. Czeremuszkin, M.R. Wertheimer, Thin Solid Films 511–512 (2006) 349.
[39] M. Yan, T.W. Kim, A.G. Erlat, M. Pellow, D.F. Foust, J. Liu, M. Schaepkens, C.M. Heller, M.A. McConnelee, T.P. Feist, A.R. Duggal, Proc. IEEE 93 (2005) 8.
[40] J. Ubrig, S. Martin, S. Cros, J.E. Bouree, J. Phys.: Conf. Ser. 100 (2008) 1.
[41] A. Ennajdaoui, J. Larrieu, S. Roualdes, J. Durand, Eur. Phys. J. Appl. Phys. 42 (2008) 9.
[42] M.B. Satterfield, P.W. Majsztrik, H. Ota, J.B. Benziger, A.B. Bocarsly, J. Polym. Sci. B: Polym. Phys. 44 (2006) 2327.
[43] L.G. Jacobsohn, M.E.H. Maia da Costa, V.J. Trava-Airoldi, F.L. Freire Jr., Diam. Relat. Mater. 12 (2003) 2037–2041.